Talanta 228 (2021) 122221

Contents lists available at ScienceDirect

Talanta

journal homepage: www.elsevier.com/locate/talanta

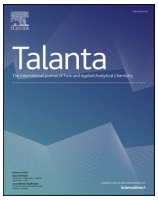

Ag_3PO_4 NP@MoS_2 nanosheet enhanced F, S-doped BN quantum dot electrochemiluminescence biosensor for K-ras tumor gene detection

Yuchen Guo [a], Yixin Nie [b], Zihui Liang [b], Wang Peilin [b], Qiang Ma [b,*]

[a] Department of Gastrointestinal Surgery, First Hospital of Jilin University, Changchun, 130000, China
[b] Department of Analytical Chemistry, College of Chemistry, Jilin University, Changchun, 130012, China

ARTICLE INFO

Keywords:
F
S-BN QD
Ag_3PO_4 NP@MoS_2 nanosheet
ECL sensor
Tumor gene detection

ABSTRACT

In this research, a novel Ag_3PO_4 NPs@MoS_2 nanosheet-based electrochemiluminescence (ECL) sensing system was developed to provide an effective method for tumor gene detection. At first, fluorine, sulfur-doped BN quantum dot (F, S-BN QD) were prepared as ECL emitter. Sulfur dopant can provide more reactive sites in the ECL reaction. Fluorine atoms in the QD structure further improved the stability of the crystal. Furthermore, Ag_3PO_4 NP@MoS_2 nanosheets were fabricated via a hydrothermal route as ECL reaction catalyst. On the one hand, Ag_3PO_4 NP@MoS_2 nanosheets promoted the generation of more oxidant of coreactant in the F, S-BN QD/H_2O_2 coreactant ECL pathway. On the other hand, the excellent conductivity of Ag_3PO_4 NP@MoS_2 nanosheets facilitated the electron transfer and effectively reduce the damage of F, S-BN QD by excessive hot electrons. Finally, the proposed biosensor was designed to accurately quantify K-ras tumor gene from 10 fM to 100 pM with a limit of detection (LOD) of 0.2 fM. The sensing system was used to detect K-ras gene in human colorectal cancer tumor and tumor-adjacent tissues samples with satisfactory results. The amplified ECL sensing strategy with Ag_3PO_4 NPs@MoS_2 nanosheet has significant potential value in the clinical detection.

1. Introduction

Tumor markers are the particular substances (e.g. protein, DNA and RNA), which exist in or are produced by tumor cells. So, tumor markers are usually in the tissues and body fluids of cancer patients [1,2]. For example, K-ras gene is a kind of important upstream gene in the RAS family. The K-ras gene mutation implied early form of cancer or adenoma, especially in the pancreatic cancer (the mutation rates up to 70~100%) [3,4]. Because tumor cells arise through the accumulation of mutations in critical proto-oncogenes and tumor suppressor genes, the K-ras gene mutation can be used as targets for pancreatic cancer diagnosis, which is also in favor of the efficient gene therapy and the development of specific anticancer drugs. Some analysis methods have been developed for tumor gene detection, including ELISA, liquid chromatography-tandem mass spectrometry, fluorescence detection, immunohistochemistry etc. [5–8] But these methods usually required time-consuming, complex operation and sophisticated sample pretreatment. Thus, it is still essential to develop a simple, rapid and accurate way for the clinical detection of K-ras gene.

ECL technology integrates the distinct advantages of electrochemistry and spectroscopy. Based on the electrogenerated chemiluminescence mode without excitation source, ECL shows quite low background noise (no auto-fluorescence and scattered light), high reproducibility and accuracy [9,10]. Therefore, ECL is a kind of idea analytical technique in the bioanalysis and clinical diagnostics. Silicon QDs have been employed as nano-emitter into the ECL sensing research in 2002 [11]. Until now, many nanoparticles (e.g. QDs, carbon dots, and metal nanoclusters) have been applied in the ECL analysis [12–14]. The nano-emitter have shown the good functional flexibility, tunable optical properties, and low cost. Meanwhile, many novel nanomaterials have developed in the sensing system as nanocarriers (e.g. MOFs and mesoporous silica beads), catalyst (e.g. Ag_3BiO_3 NPs, $NiFe_2O_4$ nanotubes, and Fe_3O_4–CeO_2 nanocomposites) and electrode surface modification materials (e.g. noble metal NPs and nanosheet), which can strengthen the ECL intensity and improve sensing sensitivity [15–21]. However, there are still several unsolved challenges in the development of ECL nanosensing system, including the low ECL efficiency of nanoparticles, the unclear ECL mechanism, and the lack of highly efficient ECL sensing mode. For example, most NPs-based ECL systems are depended on the potassium persulfate as coreactant, which could generate interference luminescence signal. Meanwhile, H_2O_2 coreactant cannot trigger nano-ECL reaction effectively.

* Corresponding author.
E-mail address: Qma@jlu.edu.cn (Q. Ma).

https://doi.org/10.1016/j.talanta.2021.122221
Received 28 December 2020; Received in revised form 3 February 2021; Accepted 13 February 2021
Available online 19 February 2021

Herein, as shown in Fig. 1, we designed an effective coreactant catalysis-amplified ECL sensing mode for the K-ras gene detection. Due to the low ECL reaction efficiency of BN QDs with hydrogen peroxide, we synthesized sulfur and fluorine doped BN QDs as ECL emitter and Ag_3PO_4 NP@MoS_2 nanosheets as coreactant catalyst. On the one hand, sulfur doping can change the surface states of BN QDs and produced new element vacancy and more reactive sites. The strong electron absorption capacity of the F atom in the QD crystal structure can reduce the energy gap between the singlet states and enhance the luminous stability of QDs. As a result, the ECL efficiency of F, S-BN QD was 1.4 times over BN QDs. On the other hand, Ag_3PO_4 NP@MoS_2 nanosheets can catalyze the coreactant ECL reaction to further enhance ECL signal. Ag_3PO_4 was an active catalyst due to the superior catalytic properties and low toxicity. However, because Ag^+ tended easily to reduce to Ag^0, the structural stability of Ag_3PO_4 was poor. So, MoS_2 nanosheets have been utilized to couple Ag_3PO_4 NP for enhancing structural stability and catalytic performance. With the engagement of MoS_2 nanosheets, Ag_3PO_4 NPs can obtain more active adsorption sites in the ECL catalysis process. With Ag_3PO_4 NP@MoS_2 nanosheets -based amplified ECL system, the ECL intensity of F, S-BN QD increased four times. The proposed biosensor can quantify the K-ras gene from 10 fM to 100 pM with a limit of detection (LOD) of 0.2 fM.

2. Experimental section

2.1. Reagents and apparatus

All reagents were of analytical grade and used directly without further purification. Boric acid, melamine, NH_4F, ammonium molybdate, thiourea, $AgNO_3$, H_2O_2, KCl and Na_2HPO_4 were purchased from Sigma. L-cysteine, glucose, HSA, GSH, ascorbic acid and ATP were purchased from HuaCheng Biological Co. All reagents were prepared using ultrapure water with a resistivity of greater than 18 MΩ cm. Human serum was obtained as a gift from the school hospital, Jilin University. All experiments were carried out at room temperature. All synthetic oligonucleotides were purchased from Sangon Biotech Co., Ltd. (Shanghai, China).

Sequences of the used oligonucleotides in present work.

Name	Sequences (5′- to -3′)
Target DNA	GTTGGAGCTAGTGGCGTAGGCAAGAGTG
Capture DNA	GCCACTAGCTCCAAC –C_6 - SH
Probe DNA	NH_2 –C_6-CACTCTTGCCTAC

Transmission electron microscopy (TEM) images were obtained with a Hitachi electron microscope operating at 200 kV acceleration voltages. Photoluminescence (PL) spectra measurements were performed on a Shimadzu RF-5301 PC spectrofluorophotometer (Shimadzu Co., Kyoto, Japan). The ultraviolet–visible (UV–vis) absorption spectra were acquired on a GBC Cintra 10e UV–vis spectrometer with a 1 cm quart cell. Fourier transform infrared spectrometry (FT-IR) was conducted on a Thermo Nicolet 360 FTIR spectrometer using KBr pellets. pH measurements were taken with a PHS-3C pH meter (Tuopu Co., Hangzhou, China). The electrochemical data were acquired with a CHI 660 B electrochemical workstation with a three –electrode system. ECL signals were acquired by a BPCL ultraweak luminescence instrument. The voltage of the photomultiplier tube (PMT) was set at 900 V during the whole process. A conventional three-electrode system was used in this system. A glassy carbon electrode (GCE) was used as the wording electrode. A platinum wire was employed as the counter electrode and an Ag/AgCl (saturated KCl) electrode as the reference electrode. In the ECL characterization experiments, the bare GCE was polished into a smooth interface by using 1.0 and 0.05 μm α-Al2O3 powder on rough paper.

2.2. Synthesis of BN QDs and F, S-doped BN QDs

F, S-doped BN QDs were synthesized by a microwave-assisted hydrothermal method. 1.6 mmol Boric acid, 0.27 mmol melamine, 0.95 mmol L-cysteine and 2.5 mmol NH_4F were dissolved in ultrapure water. F, S-doped BN QDs were obtained under the 1000 Hz reflection frequency of microwave, 60 min and 180 °C. To remove excess precursors, the solution was centrifuged at 5000 rpm for 5 min and washed two times. The product was preserved in 4 °C refrigerator. For comparison, we also prepared the BN QDs with boric acid and melamine as precursors under the similar conditions according to the previous reports. Briefly, 1.6 mmol boric acid and 0.27 mmol melamine were dissolved in 10 mL H_2O. Under the microwave-assisted hydrothermal condition (120 °C, 70 min), the mixture was reacted to synthesize BN QDs. To remove excess precursor, the solution was centrifuged at 12,000 rpm for 20 min and washed two times. The BN QDs product was dried and dispersed in 15 mL ultrapure water under ultrasound.

2.3. Synthesis of Ag_3PO_4 NP@MoS_2 nanosheets

Firstly, MoS_2 nanosheets were synthesized by the hydrothermal method. 20 mg of ammonium molybdate and 40 mg of thiourea were dissolved in 12 mL H_2O. After stirred for 5 min, the mixtures were heated into a 20 mL Teflon-lined autoclave at 200 °C for 12 h, followed by natural cooling to room temperature. The solution was centrifuged at 12,000 rpm for 20 min and washed two times. Then, MoS_2 nanosheets product was dried for the next synthesis process. Secondly, 0.0105 g MoS_2 nanosheets was mixed at 25 mL solution. 1.5 mmol $AgNO_3$ and 0.5 mmol Na_2HPO_4 were dissolved in 25 mL water respectively. Then, $AgNO_3$ solution was added into the MoS_2 nanosheets solution drop by drop. Finally, Na_2HPO_4 solution was added into the mixture drop by drop. Under dark conditions, the above solution was stirred for 1.5 h. After centrifuged at 12,000 rpm for 20 min and washed two times, the Ag_3PO_4 NP@MoS_2 nanosheets product was dried and preserved.

2.4. K-ras gene detection

For ECL detection, a sandwich immunoassay mode was designed. 100 μL of 10 μM capture DNA was injected into 1 mL Ag_3PO_4 NP@MoS_2 nanosheets solution. Then, the solution was incubated for 2 h to form Ag_3PO_4 NP@MoS_2 nanosheet/capture DNA. The above solution was dialyzed for 4 h under stirring to remove the unreacted DNA. F, S-doped

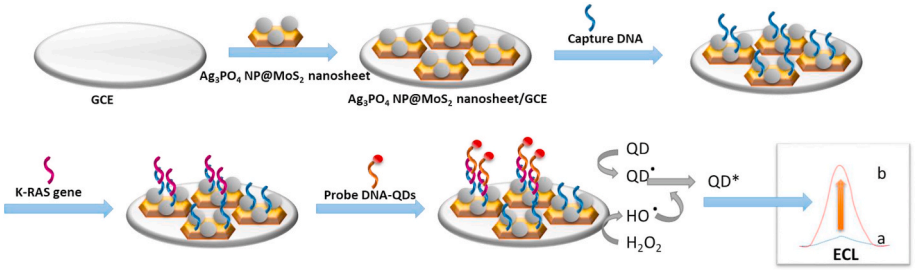

Fig. 1. Schematic illustration of Ag_3PO_4 NP@MoS_2 nanosheet enhanced F, S-doped BN QD-based ECL biosensor.

BN QDs and probe DNA were connected by covalent link carboxyl and amino. 30 μL 10 mmol/L EDC and 10 μL 10 mmol/L NHS were added into 2 mL F, S-doped BN QDs to activate carboxyl group. Then, 15 μL 10 μmol/L probe DNA was added and stirred for 2 h. Finally, the solution was dialyzed for 3 h to remove the unreacted small molecules.

In the sensing process, Ag_3PO_4 NP@MoS_2 nanosheet/capture DNA solution was dropped on GCE and blocked with 20 μL of 2 wt% bovine serum albumin solution at 37 °C. After dried in N_2, the above working electrode was incubated with 200 μL different concentrations of target DNA for 10 min at 66 °C. Then, the electrode was washed with Tris-HCl buffers (pH 7.4) to remove excess target DNA. Afterward, the above electrode was incubated with 200 μL F, S-doped BN QD/probe DNA for 10 min at 66 °C and cooled to room temperature. When the hybridization was accomplished, Tris-HCl buffers was used to washed the electrode extensively. Finally, the ECL intensity was recorded in phosphate buffer solution (0.1 M, pH 7.4) containing 0.01 M H_2O_2 from −2 to 0 V (versus Ag/AgCl) at the scan rate of 100 mV/s. The voltage of the photomultiplier tube (PMT) was set at 900 V in the process of detection. The human colorectal cancer tumor and tumor-adjacent tissues samples was got from the first hospital of Jilin University. The ECL signals were detected in the tissue lysate according to the above procedure.

3. Results and discussion

3.1. Characterization of F, S-doped BN QDs and Ag_3PO_4 NP@MoS_2 nanosheets

Fig. 2 (A) was TEM image of F, S-doped BN QDs. The morphology of F, S-doped BN QDs was uniform. The size of QDs was ca. 3 nm. The morphology and microstructure of Ag_3PO_4 NP@MoS_2 nanosheets were investigated by the field emission scanning electron microscope (SEM). In Fig. 2 (B), MoS_2 nanosheets presented a regular hexagon sheet structure. It clearly showed that some Ag_3PO_4 NPs was loaded on the surface of MoS_2 nanosheets. The UV–vis and PL spectrum of F, S-doped BN QDs presented the relation between the crystal structure of F, S-doped BN QDs and their optical properties. The UV–vis absorption spectra of BN QDs and F, S-doped BN QDs were showed in Fig. 3 (A). The UV–vis spectra of the BN QDs showed the absorption peak centered at 230 nm. The doping of fluorine and sulfur caused a blue shift of the absorption peak. The absorption peak of F, S-doped BN QDs at 240 nm was due to the presence of sulfur atom in crystal structure. The interaction of the major absorbing species on the sp^2 platform with the sulfur atom caused a shift in absorption spectrum. It also indicated that the doping of fluorine and sulfur reduce band gap of the BN QDs. In Fig. 3 (B), F, S-doped BN QDs showed the excitation-dependent emission properties with different excitation wavelength. The PL spectrum of F, S-doped BN QDs was obtained at different excitation wavelength from 325 nm to 500 nm. The emission of F, S-doped BN QDs varied from 425 nm to 550 nm. It was due to different function groups on the surface of F, S-doped BN QDs. The results indicated that the doping of fluorine and sulfur in the synthesis process of S-BN QDs can further regulate more luminescence canters, which caused excitation dependence of F, S-doped BN QDs.

3.2. The ECL behavior of F, S-doped BN QDs

Fig. 4 (A) showed the comparison of ECL spectrum and PL spectrum of F, S-doped BN QDs. The maximum PL emission peak of F, S-doped BN QDs was 460 nm, and the ECL emission peak of F, S-doped BN QDs were 620 nm. The significant red shift of ECL emission peak was due to the ECL emission mechanism. Unlike the photoluminescence generation process, electron transfer occurred to produce the excited state of QDs in the ECL reaction. The ECL generation was dependent on the electron transfer process between the electrode, coreactant and QDs surface. Generally, the band gap of QDs surface state was narrower than that of core. Therefore, the large red shift in the ECL peak from the photoluminescence peak can be observed. Fig. 4 (B) showed that the cyclic voltammetry was performed with a supporting electrolyte of 0.01 mol/L H_2O_2. There was an oxidation peak at 0.175 V in the F, S-doped BN QDs/H_2O_2 system. The current changing confirmed the ECL reaction between F, S-doped BN QDs and H_2O_2. F, S-doping provided more surface capturing centers of excitons on the QDs surface. Therefore, the F, S-doped BN QDs can capture more holes from co-reactant and generated strong ECL intensity. The ECL intensity of BN QDs and F, S-doped BN QDs with H_2O_2 was compared. As a result, the ECL intensity of F, S-doped BN QDs increased 1.4 times to BN QDs. The detailed mechanism for ECL generation of F, S-doped BN QDs can be described with the equations below:

$$H_2O_2 + e^- \rightarrow OH^- + OH^{\cdot} \quad (1)$$

$$\text{F, S-doped BN QD} + e^- \rightarrow \text{F, S-doped BN QD}^{\cdot-} \quad (2)$$

$$\text{F, S-doped BN QD}^{\cdot-} + OH^{\cdot} \rightarrow \text{F, S-doped BN QD*} + OH^- \quad (3)$$

$$\text{F, S-doped BN QD*} \rightarrow \text{F, S-doped BN QD} + h\nu \quad (4)$$

Firstly, H_2O_2 was reduced to produce a strong oxidizing species ($OH^{\cdot}$). The oxidizing species reacted with QDs by injecting a hole into the HOMO orbital and produced an excited state of QDs (F, S-doped BN QD*), which then relaxed to the ground state and light emission.

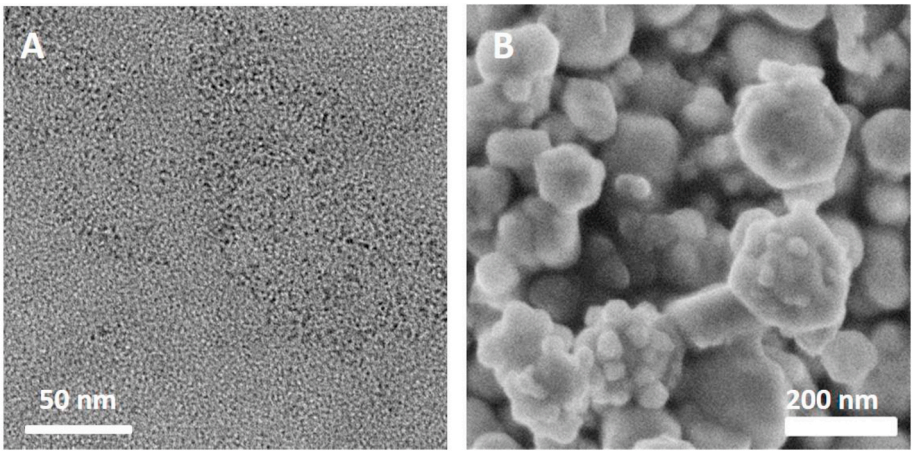

Fig. 2. (A) The TEM photo of F, S-doped BN QDs and (B) The SEM photo of Ag_3PO_4 NP@MoS_2 nanosheets.

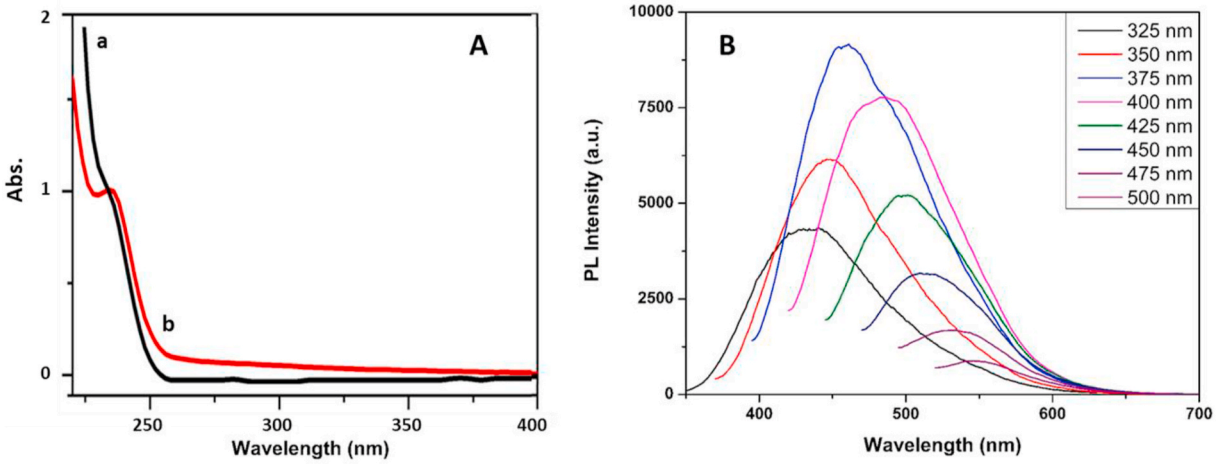

Fig. 3. (A) UV–vis absorption spectra of BN QDs (a) and F, S-doped BN QDs (b). (B) Fluorescence spectra of F, S-doped BN QDs in different excitation wavelengths.

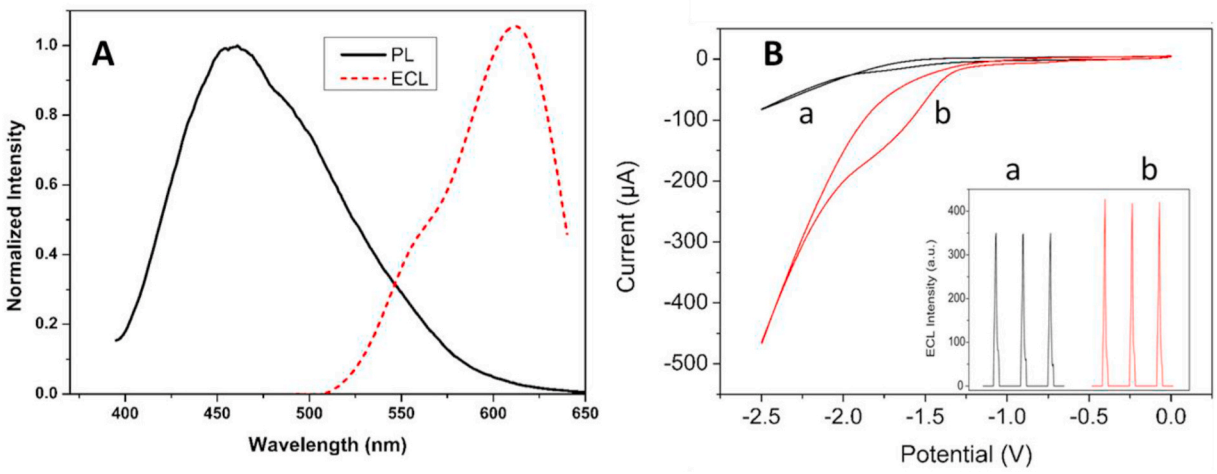

Fig. 4. (A) ECL spectrum and PL spectrum of F, S-doped BN QDs. (B) The cyclic voltammograms of BN QDs (a) and F, S-doped BN QDs (b) with H_2O_2. Insert is the ECL intensity of BN QDs (a) and F, S-doped BN QDs (b).

3.3. Ag_3PO_4 NP@MoS_2 nanosheet-amplified ECL mechanism

Fig. 5 A and B were the ECL-potential curves and the corresponding ECL intensity of F, S-doped BN QDs with Ag_3PO_4 NP@MoS_2 nanosheet, respectively. Compared with F, S-doped BN QDs original ECL signal, Ag_3PO_4 NP@MoS_2 nanosheet significantly increased the ECL intensity.

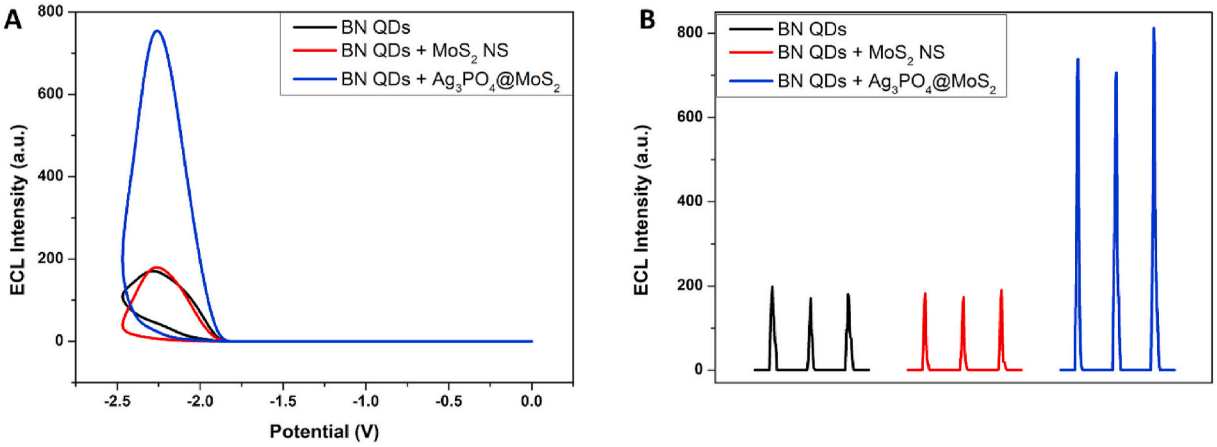

Fig. 5. Comparison of ECL potential (A) and ECL intensity (B) of F, S-doped BN QDs, F, S-doped BN QDs with MoS_2 nanosheet, and F, S-doped BN QDs with Ag_3PO_4 NP@MoS_2 nanosheet.

It confirmed the catalytic effect of Ag_3PO_4 NP@MoS_2 nanosheet with the unchanged potential position. Much ·OH were generated by catalysis of Ag_3PO_4 NP@MoS_2 nanosheet. In the next step, more ·OH promoted QDs to emit stronger ECL signal. Moreover, the cathode in the ECL system can continuously supply electrons to reductive Ag_3PO_4 NP on the MoS_2 nanosheet. As a result, Ag_3PO_4 NP@MoS_2 nanosheet was reduced to the original valence state and generate ·OH continuously. The mechanism reactions were as follows:

$$H_2O_2 + e^- \rightarrow OH^- + OH \quad (5)$$

$$Ag_3PO_4 \text{ NP@}MoS_2 \text{ nanosheet} + e^- \rightarrow \text{reductive } Ag_3PO_4 \text{ NP@}MoS_2 \text{ nanosheet} \quad (6)$$

$$\text{F, S-doped BN QD} + OH^{\cdot} + e- \rightarrow \text{F, S-doped BN QD*} + OH\text{-} \quad (7)$$

$$\text{F, S-doped BN QD*} \rightarrow \text{F, S-doped BN QD} + h\nu \quad (8)$$

In order to show the Ag_3PO_4 NP@MoS_2 nanosheet-based amplified ECL performance, MoS_2 nanosheet without Ag_3PO_4 NP was investigated. As shown in Fig. 5, the ECL intensity of F, S-doped BN QDs and F, S-doped BN QDs on the MoS_2 nanosheet were similar. In comparison, the ECL intensity of F, S-doped BN QDs with Ag_3PO_4 NP@MoS_2 nanosheet increased up to 400%. The results exhibited the catalytic effect of Ag_3PO_4 NPs on the MoS_2 nanosheet. Meanwhile, MoS_2 nanosheet improved the stability and catalytic activity of Ag_3PO_4 NPs. Moreover, the effect of different concentrations of Ag_3PO_4 NP@MoS_2 nanosheet on the ECL enhancement were investigated (as shown in Fig. 6 A). When Ag_3PO_4 NP@MoS_2 nanosheet was introduced into the electrode surface, the ECL of QDs increased. The ECL response of QDs reached to the maximum when 60 mg/L Ag_3PO_4 NP@MoS_2 nanosheet was added. Since the potential peak position did not change with the addition of MoS_2 nanosheet or Ag_3PO_4 NP@MoS_2 nanosheet, Ag_3PO_4 NP@MoS_2 nanosheet acted as catalysts in the light-emitting process of F, S-doped BN QDs. The results confirmed that the catalytic effect of MoS_2 nanosheet on hydrogen peroxide was far less than the catalytic effect of Ag_3PO_4 NP@MoS_2 nanosheet. Meanwhile, MoS_2 nanosheet improved the stability and catalytic activity of Ag_3PO_4 NPs. The synergistic catalytic effect of Ag_3PO_4 NPs and MoS_2 nanosheet played a decisive role in ECL enhancement. The correlations between the ECL intensity of F, S-doped BN QDs and Ag_3PO_4 NP@MoS_2 nanosheet shown in Fig. 6 (B). The ECL enhancement were significantly correlated with the catalysis extent of Ag_3PO_4 NP@MoS_2 nanosheet. And the ECL amplification was not related to MoS_2 nanosheet. The reliability of the catalytic effect of Ag_3PO_4 NP@MoS_2 nanosheet was investigated with a series of parallel experiments test in Fig. 6 (C). The above results indicated the catalysis ability of Ag_3PO_4 NP@MoS_2 nanosheet in the ECL reaction. When much Ag_3PO_4 NP@MoS_2 nanosheet were coated on the electrode, an ECL quenching effect can be observed. It was because that the co-reactant was directly consumed by the too strong catalytic ability. Therefore, 60 mg/L Ag_3PO_4 NP@MoS_2 nanosheet was selected to construct the ECL sensor.

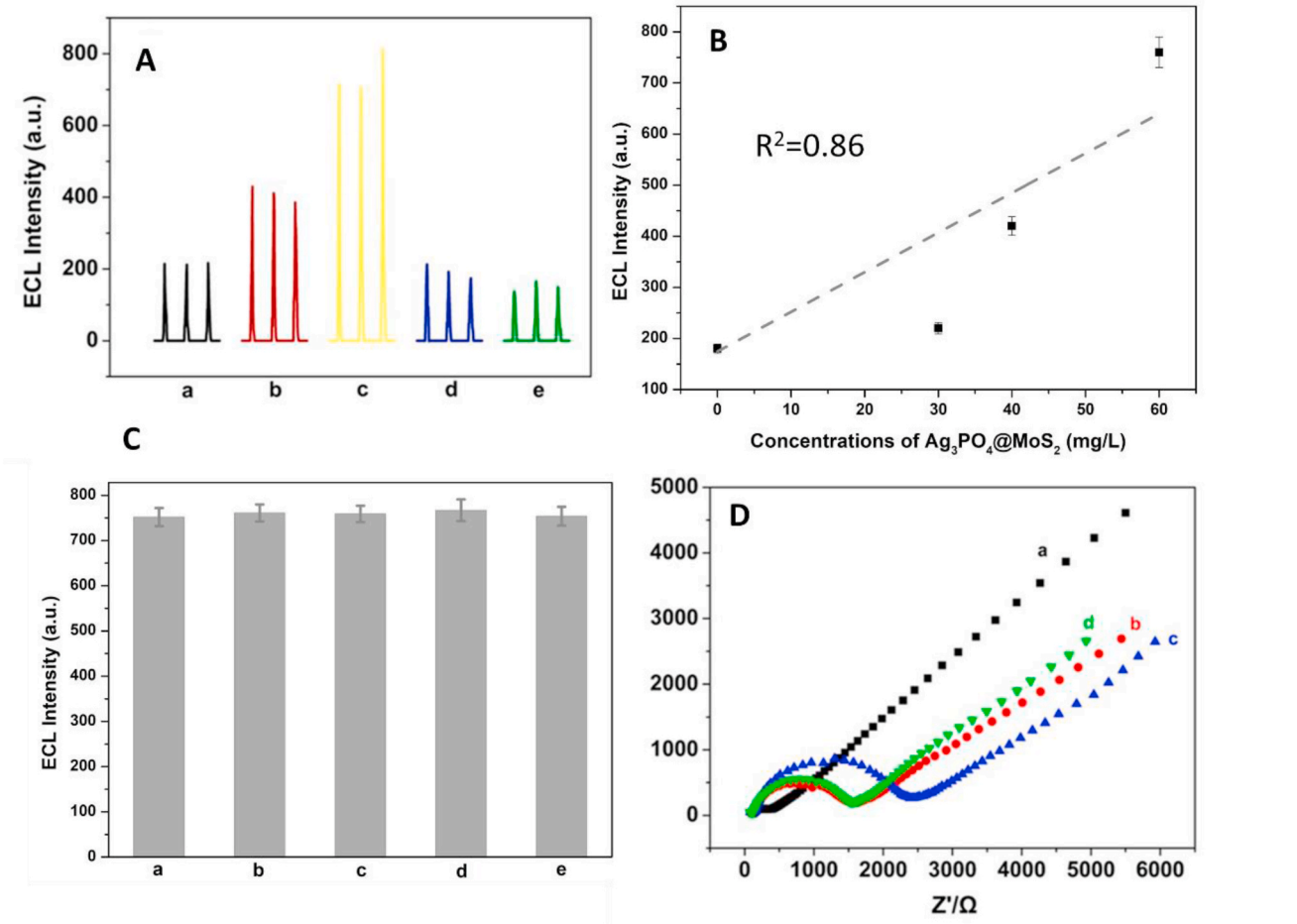

Fig. 6. (A) The ECL responses of F, S-doped BN QDs with different concentrations of Ag_3PO_4 NP@MoS_2 nanosheet (a 30 mg/L, b 40 mg/L, c 60 mg/L, d 100 mg/L, e 300 mg/L). (B) The correlation analysis of the ECL intensity of F, S-doped BN QDs and Ag_3PO_4 NP@MoS_2 nanosheet. (C) The parallel experiments test for the ECL enhancement with Ag_3PO_4 NP@MoS_2 nanosheet. (D) EIS of (a) GCE, (b) capture DNA/Ag_3PO_4 NP@MoS_2 nanosheet/GCE, (c) target DNA/capture DNA/Ag_3PO_4 NP@MoS_2 nanosheet/GCE, and (d) F, S-doped BN QDs/probe DNA/target DNA/capture DNA/Ag_3PO_4 NP@MoS_2 nanosheet/GCE.

3.4. K-ras detection

Fig. 6 (D) showed the electrochemical impedance spectroscopy (EIS) changes in the sensor construction process. The electron transfer resistance (Ret) of the bare GCE (curve a) was very small. The semicircle diameter of capture DNA/Ag_3PO_4 NP@MoS_2 nanosheet/GCE was increased clearly (curve b). When target DNA were captured on the surface of GCE (curve c), the Ret increased gradually due to the non-conductivity of DNA. When F, S-doped BN QDs/probe DNA were captured, the Ret decreased. It was caused by the electrical conductivity of F, S-doped BN QDs. The above results indicated the ECL sensor is constructed successfully. Fig. 7 displayed the corresponding ECL intensity change with the addition of K-ras gene. The linear equation between the logarithm of gene concentration and the ECL intensity was I = 70.774 log [K-ras gene] + 243.66. The detection linear range from 10 fM to 100 pM. The detection limit was as low as 0.2 fM we also evaluated the selectivity of the sensing system. The sensor showed superior selectivity in 100-fold concentrations of glucose, HSA, GSH, ascorbic acid and ATP. Furthermore, the precision and accuracy of the sensor is investigated and recorded in Fig. 7 (C). The ECL sensor showed good stability in both intra-assays (RSD 2.98%) and inter-assays (RSD 3.12%). Table 1 listed the detection results of the K-ras gene in human colorectal cancer and tumor-adjacent tissues using the standard addition method. The recovery rates were 101%–124% and the RSD was less than 4%. The results revealed that overexpression of K-ras gene was quite higher in the colorectal tumor than tumor-adjacent tissues. It indicated the reliability and accuracy of the K-ras gene detection in actual application.

Table 1
Results of determination of K-ras in human colorectal cancer tumor and tumor-adjacent tissues.

Sample	Original (pM)	Spiked (pM)	Founded (pM)	Recovery (%)	RSD (%) (n = 3)
tumor 1	0.12	0.5	0.74	124.0	2.57
tumor-adjacent 1	0.002	0.5	0.52	104.0	2.61
tumor 2	0.36	0.5	0.95	118.0	3.78
tumor-adjacent 2	0.04	0.5	0.55	102.0	1.09
tumor 3	1.43	1.0	2.46	102.9	1.85
tumor-adjacent 3	0.05	1.0	1.06	101.0	3.04

4. Conclusions

In this work, we have developed the Ag_3PO_4 NP@MoS_2 nanosheet-amplified F, S-doped BN QDs ECL sensing mode. With the F and S doping, F, S-doped BN QDs had high ECL efficiency. Meanwhile, on the

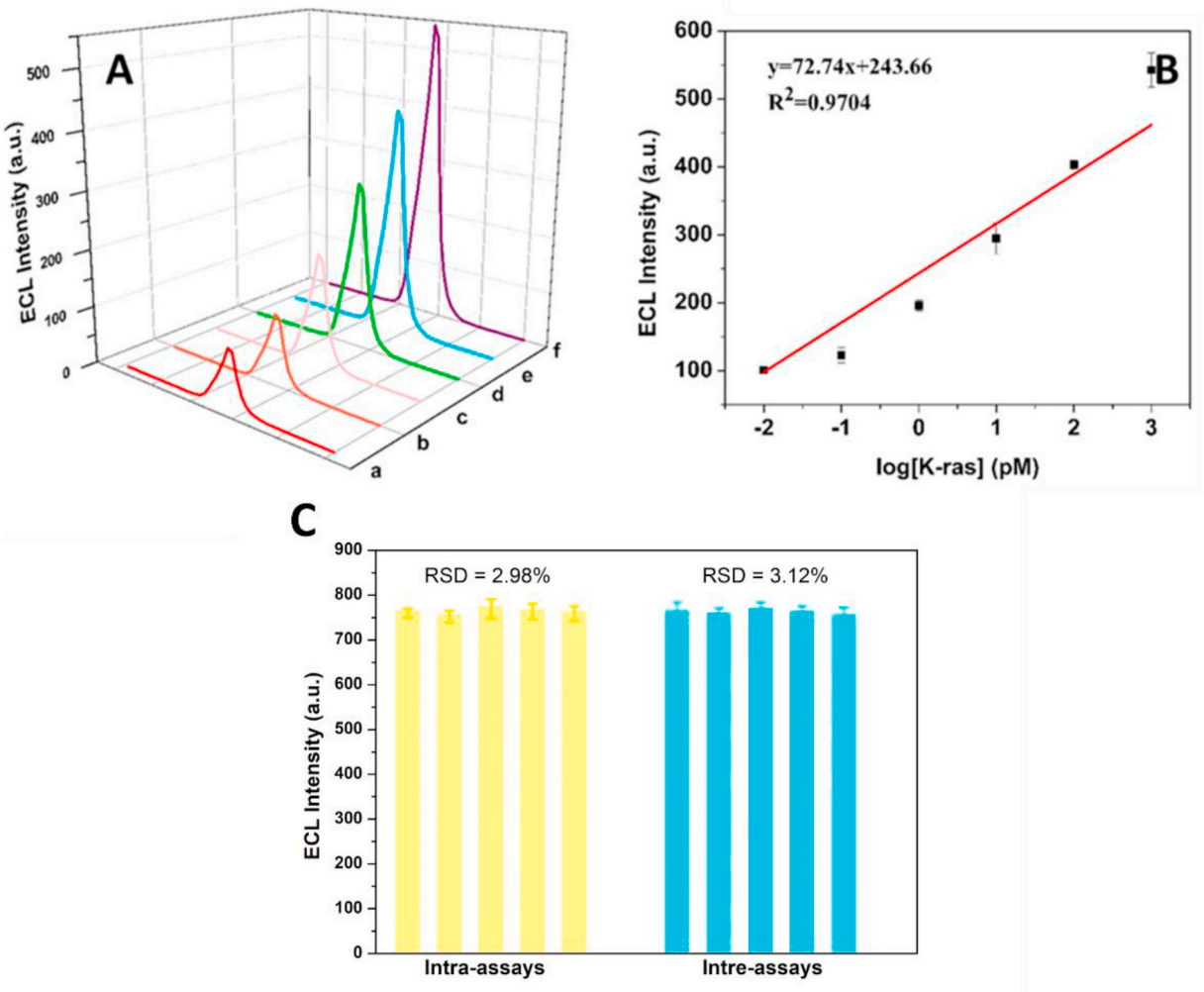

Fig. 7. (A) The ECL responses with different concentrations of K-ras gene (from 10 fM to 100 pM). (B) Calibration plot of the ECL intensity and logarithm of K-ras gene concentrations. (C) The repeatability of the sensor was investigated by intra- and inter-assays.

modified electrode with Ag_3PO_4 NP@MoS_2 nanosheet, hydrogen peroxide can be produced effectively. As expected, the ECL signal of QDs can be enhanced. The Ag_3PO_4 NP@MoS_2 nanosheet-amplified F, S-doped BN QDs-based sensor do not only overcome the limitation of the low ECL efficiency of BN QDs, but also greatly improved the sensitivity of ECL detection. The proposed biosensor accurately quantified K-ras gene from 10 fM to 100 pM with a limit of detection of 0.2 fM. This method provides a meaningful sensing system for the testing of tumor gene.

CRediT author statement

Yuchen Guo: Conceptualization, Data curation, Formal analysis, Writing – original draft. Yixin Nie: Investigation. Zihui Liang: Methodology. Wang Peilin: Investigation, Qiang Ma: Supervision, Project administration, Resources, Writing – review & editing.

Declaration of competing interest

The authors declare that they have no known competing financial interests or personal relationships that could have appeared to influence the work reported in this paper.

Acknowledgements

The present work was supported by Natural Science Foundation of Jilin Province (No. 20200201301JC).

References

[1] J.J. Havel, D. Chowell, T.A. Chan, The evolving landscape of biomarkers for checkpoint inhibitor immunotherapy, Nat. Rev. Canc. 19 (2019) 133–150.
[2] M. Regouc, G. Belge, A. Lorch, K.P. Dieckmann, M. Pichler, Non-coding micrornas as novel potential tumor markers in testicular cancer, Cancers 12 (2020) 749.
[3] A. Zhang, R. Wang, K. Sun, Z. Jia, H. Xie, Diagnosis value of detection K-ras gene mutations in patients with gastric cancer, Adv. Mater. Res. 396–398 (2012) 1470–1474.
[4] R. D'Agata, N. Bellassai, M. Allegretti, A. Rozzi, S. Korom, A. Manicardi, E. Melucci, E. Pescarmona, R. Corradini, P. Giacomini, G. Spoto, Direct plasmonic detection of circulating RAS mutated DNA in colorectal cancer patients, Biosens. Bioelectron. 170 (2020), 112648.
[5] N. Bagherlou, S. Farajnia, S. Zahri, A.D. Tabrizi, A. Nazari, Prevalence of K-ras mutations and CA125 tumor marker in patients with ovarian carcinoma, Casp. J. Int. Med. 11 (2020) 75–82.
[6] M.B. Cammarata, C.L. Schardon, M.R. Mehaffey, J. Rosenberg, J. Singleton, W. Fast, J.S. Brodbelt, Impact of G12 mutations on the structure of K-ras probed by ultraviolet photodissociation mass spectrometry, J. Am. Chem. Soc. 138 (2016) 13187–13196.
[7] M.B. Wabuyele, H. Farquar, W. Stryjewski, R.P. Hammer, S.A. Soper, Y.-W. Cheng, F. Barany, Approaching real-time molecular diagnostics: single-pair fluorescence resonance energy transfer (spFRET) detection for the analysis of low abundant point mutations in K-ras oncogenes, J. Am. Chem. Soc. 125 (2003) 6937–6945.
[8] C. Glorieux, P. Huang, Regulation of CD137 expression through K-Ras signaling in pancreatic cancer cells, Canc. Commun. 39 (2019) 386.
[9] Y. Liu, M. Wang, Y. Nie, Q. Zhang, Q. Ma, Sulfur regulated boron nitride quantum dots electrochemiluminescence with amplified surface plasmon coupling strategy for BRAF gene detection, Anal. Chem. 91 (2019) 6250–6258.
[10] Y. Fu, Q. Ma, Recent developments in electrochemiluminescence nanosensors for cancer diagnosis applications, Nanoscale 12 (2020) 13879–13898.
[11] Z. Ding, B.M. Quinn, S.K. Haram, L.E. Pell, B.A. Korgel, A.J. Bard, Electrochemistry and electrogenerated chemiluminescence from silicon nanocrystal quantum dots, Science 296 (2002) 1293–1297.
[12] Y. Liu, Y. Nie, M. Wang, Q. Zhang, Q. Ma, Distance-dependent plasmon-enhanced electrochemiluminescence biosensor based on MoS2 nanosheets, Biosens. Bioelectron. 148 (2020) 111823.
[13] Y. Chen, Y. Cao, C. Ma, J.-J. Zhu, Carbon-based dots for electrochemiluminescence sensing, Mater. Chem. Front. 4 (2020) 369–385.
[14] Y. Jia, L. Yang, J. Xue, N. Zhang, D. Fan, H. Ma, X. Ren, L. Hu, Q. Wei, Bioactivity-protected electrochemiluminescence biosensor using gold nanoclusters as the low-potential luminophor and Cu2S snowflake as Co-reaction accelerator for procalcitonin analysis, ACS Sens. 4 (2019) 1909–1916.
[15] X. Yang, Y.-Q. Yu, L.-Z. Peng, Y.-M. Lei, Y.-Q. Chai, R. Yuan, Y. Zhuo, Strong electrochemiluminescence from MOF accelerator enriched quantum dots for enhanced sensing of trace cTnI, Anal. Chem. 90 (2018) 3995–4002.
[16] L. Chu, G. Zou, X. Zhang, Electrogenerated chemiluminescence sensor for formaldehyde based on $Ru(bpy)_3^{2+}$-doped silica nanoparticles modified Au electrode, Mater. Sci. Eng. C 32 (2012) 2169–2174.
[17] Y. Zhou, M. Chen, Y. Zhuo, Y. Chai, W. Xu, R. Yuan, In situ electrodeposited synthesis of electrochemiluminescent Ag nanoclusters as signal probe for ultrasensitive detection of cyclin-D1 from cancer cells, Anal. Chem. 89 (2017) 6787–6793.
[18] H. Liao, C. Jin, Y. Zhou, Y. Chai, R. Yuan, Novel ABEI/dissolved O_2/Ag_3BiO_3 nanocrystals ECL ternary system with high luminous efficiency for ultrasensitive determination of MicroRNA, Anal. Chem. 91 (2019) 11447–11454.
[19] J. Wang, J. Song, H. Zheng, X. Zheng, H. Dai, Z. Hong, Y. Lin, Application of $NiFe_2O_4$ nanotubes as catalytically promoted sensing platform for ratiometric electrochemiluminescence analysis of ovarian cancer marker, Sensor. Actuator. B Chem. 288 (2019) 80–87.
[20] Y. Li, Y. Chu, Y. Li, C. Ma, L. Li, A novel electrochemiluminescence biosensor: inorganic-organic nanocomposite and $ZnCo_2O_4$ as the efficient emitter and accelerator, Sensor. Actuator. B Chem. 303 (2020), 127222.
[21] X. Liu, Q. Wang, J. Chen, X. Chen, W. Yang, Ultrasensitive electrochemiluminescence biosensor for the detection of tumor exosomes based on peptide recognition and luminol-AuNPs@g-C_3N_4 nanoprobe signal amplification, Talanta 221 (2021) 121379.